



# Modified Sucrose Biochar Goethite ( $\alpha$ -FeOOH): A Potential Adsorbent for Methylene Blue Removal

Van-Truc Nguyen<sup>1</sup> · Nguyen Duy Dat<sup>2</sup> · Quoc-Hoang Do<sup>1</sup> · Vu-Anh Le<sup>3</sup> · Quoc-Minh Truong<sup>4</sup> · Thanh-Binh Nguyen<sup>5</sup> · Anh Thi Kim Tran<sup>2</sup> · My Linh Nguyen<sup>2</sup> · Nhung Thi-Tuyet Hoang<sup>2</sup> · Tran Thi Ai My<sup>6</sup> · Thi-Dieu-Hien Vo<sup>3</sup> 

Received: 19 April 2024 / Revised: 23 June 2024 / Accepted: 20 July 2024

© The Author(s), under exclusive licence to Korean Institute of Chemical Engineers, Seoul, Korea 2024

## Abstract

The primary purpose of this study is to synthesize biochar (Fe-SB) derived from sucrose through hydrothermal carbonization coupling with goethite activation and utilize it as an adsorbent to remove methylene blue (MB). FTIR, SEM, and BET were used to analyze the biochar characterization. Factors affecting the adsorption of MB on Fe-SB, including temperature, pH, salt, and different water sources, were also meticulously investigated. SEM results indicate that the morphology of the biochar derived from sucrose has a spherical shape, and the goethite crystal has a needle-like structure that successfully deposits on the adsorbent. The specific surface area of Fe-SB is 568 m<sup>2</sup>/g and contains enormous functional groups of O–H, C=C, and C–O. In the condition of pH 8, Fe-SB had a maximum adsorption capability of 476.2 mg/g. The adsorption capacity of biochar for MB removal consists of various adsorption mechanisms. In conclusion, Fe-SB, a novel material, pinpoints a promising and environmentally friendly adsorbent for the removal of MB from aquatic environment.

**Keywords** Biochar · Sucrose · Goethite · Adsorption · Methylene blue (MB)

✉ Thi-Dieu-Hien Vo  
vtdhien@ntt.edu.vn

Van-Truc Nguyen  
nvtruc@sgu.edu.vn

Nguyen Duy Dat  
datnd@hcmute.edu.vn

Quoc-Hoang Do  
quochoangdo@gmail.com

Vu-Anh Le  
levuanh1995544@gmail.com

Quoc-Minh Truong  
quocminht@tdmu.edu.vn

Thanh-Binh Nguyen  
ntbinh179@nkust.edu.tw

Anh Thi Kim Tran  
anhhtt@hcmute.edu.vn

My Linh Nguyen  
nhunghtt@hcmute.edu.vn

Nhung Thi-Tuyet Hoang  
linhnm@hcmute.edu.vn

Tran Thi Ai My  
aimy.chem@hueuni.edu.vn

- 1 Faculty of Environment, Saigon University, Ho Chi Minh City 700000, Vietnam
- 2 Faculty of Chemical & Food Technology, Ho Chi Minh City University of Technology and Education, Thu Duc, Ho Chi Minh City, Vietnam
- 3 Institute of Applied Technology and Sustainable Development, Nguyen Tat Thanh University, Ho Chi Minh City 700000, Vietnam
- 4 Department of Management Science, Thu Dau Mot University, Binh Duong 75000, Vietnam
- 5 Institute of Aquatic Science and Technology, National Kaohsiung University of Science and Technology, Kaohsiung City 81157, Taiwan
- 6 Department of Chemistry, University of Sciences, Hue University, Hue 530000, Vietnam

## Introduction

Dyes that appear in wastewater systems can be associated with some industrial activities like the paper industry, leather industry, and paint powder from the colorful products they create using dyes and pigments [1, 2]. There are more than 700,000 tons of dyes which are produced each year, and due to ineffective dyeing methods, almost 200,000 tons of synthetic dyes have been discharged into a water source [3]. Wastewater contains dyes that are extremely hard to treat and harmful by their toxic and carcinogenic features [4]. Therefore, if the quality of outlet wastewater containing dyes does not have a sufficient treatment method before being discharged out to the environment, it could change the color of the water and affect aqueous creatures, as well as human health by accumulating in our bodies [5–7]. One of the dyestuffs usually used in the textile industry in Vietnam can be named is the thiazine dye methylene blue (MB). When exposed to MB, the human body will suffer some changes, including vomit, high blood pressure (causing cardiovascular disease), headaches, and shortness of breath [8]. Moreover, methylene blue can cause cancer as indicated by many previous studies; particularly, the study by Auerbach et al. [9] has found that the incidences of pancreatic islet cell adenoma and adenoma or carcinoma (combined) were increased in all groups of male rats that were exposed to MB. On the other hand, many treatment methods and technologies were used aim to remove dyes in wastewater, typically membrane filtration [10, 11], ion exchange, electrochemistry, flocculation, microbes, sludge, coagulation, electrolysis, anaerobic hydrolysis, and advanced oxidation process [11–15], but the most capable and cost-effective method is adsorption [16–19].

Biochar is an adsorbent that has a wide range of precursor materials like industrial waste [20], agricultural by-products [21–23], such as studies on using eggplant peel as a biological adsorbent have demonstrated its effectiveness in treating domestic wastewater contaminated with oil [24], livestock manure [25, 26], and sludge [27]. Moreover, activating-biochar is considered a potential adsorbent because of its high porosity [23, 28], and high internal and external surface area [28], and contain an enormous number of functional groups [20, 23]. Sucrose has been widely used as a precursor material to synthesize adsorbent material due to its marvelous features like high specific surface area, multiple surface functional groups, and the like [29, 30]. For instance, activated carbon made from sucrose and KOH chemical activation performs incredibly well at removing methylene blue, with a maximum capacity of 704.2 mg/g [31]. Moreover, the activated carbon has achieved a huge BET surface area of 1534 m<sup>2</sup>/g and a

volume of 0.765 cm<sup>3</sup>/g. In another study, low-cost-sugar-based materials were synthesized using glucose, sucrose, and molasses and utilizing them to remove metals in water [32]. The sucrose-based adsorbent exhibited its ability for heavy metal ions removal in water, particularly As (V), Zn (II), and Cd (II). Besides, a common iron oxyhydroxide found in sediments, rocks, and soils called goethite ( $\alpha$ -FeOOH) is very stable in the natural world. Recently,  $\alpha$ -FeOOH has been discovered to be an excellent material for removing metal ions from water due to its reasonable cost, naturally abundant, nontoxicity, high specific surface area, and compatible structure [33]. In another study, Zhang et al. [34] prepared an adsorbent through one-step hydrothermal supported by  $\alpha$ -FeOOH and manipulated it to remove Pb<sup>2+</sup>. The adsorbent equilibrium adsorption ability achieves up to 103.04 mg/g. Moreover, the adsorbent still retains its great removal performance of 77.3 mg/g after five reused cycles. It shows that the  $\alpha$ -FeOOH is a great material to synthesize biochar-activated carbon.

For the aforementioned reasons, this study focuses on creating a novel composite of Fe-SB to remove MB from the water and evaluate its potential by analyzing the affecting parameters, including effects of adsorbent dosage, initial pH, initial MB concentration, reaction temperature, and contact time. Besides, the Fe-SB was characterized using BET, FTIR, and SEM analysis methods. Based on the results from the experiment and material characterization, the adsorption mechanism, kinetics, and equilibrium isotherm are also analyzed.

## Materials and Methods

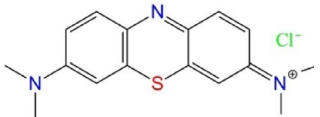
### Chemicals

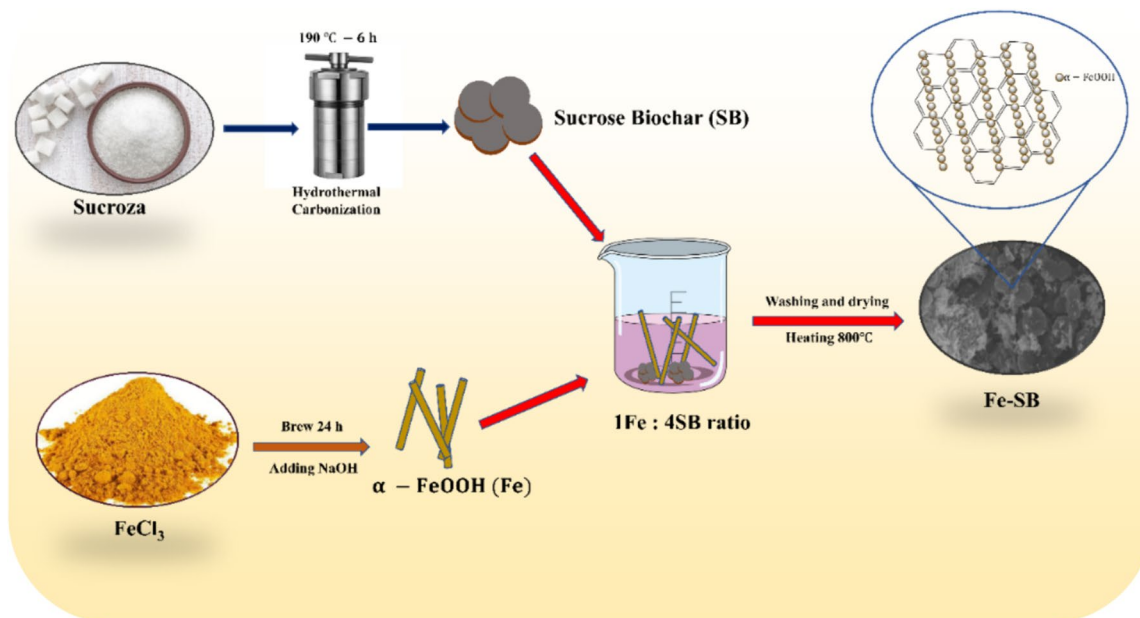
Sucrose (C<sub>12</sub>H<sub>22</sub>O<sub>11</sub>), Sulfuric acid (H<sub>2</sub>SO<sub>4</sub>), Hydrochloric acid (HCl), Sodium hydroxide (NaOH), Methylene Blue (C<sub>16</sub>H<sub>18</sub>ClN<sub>3</sub>S), Ethanol (C<sub>2</sub>H<sub>5</sub>OH), and Iron (III) chloride hexahydrate (FeCl<sub>3</sub>·6H<sub>2</sub>O) were provided from Beijing Chemical Co. Ltd., China and qualified as an analytical grade. All solutions were prepared using double distilled (DI) water during the entire experiment. The characteristics of methylene blue are shown in Table 1.

### Preparation of Hydrochar and Biochar

Hydrothermal carbonization experiments were conducted using autoclave reactor instrument equipment. For each run, 30 g of sucrose and 150 mL of DI water (1:3, w/w) were transferred to the reaction vessel with the temperature heated to 190 °C for 6 h in a drying oven. Then, the hydrochar was dried in an oven at 60 °C overnight before being soaked in

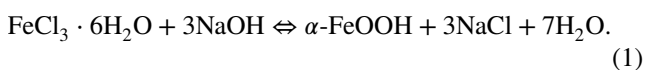
**Table 1** Properties of methylene blue

Molecular formula	Molecular structure	p $K_a$	Solubility (25 °C)	Molar mass (g/mol)
$C_{16}H_{24}ClN_3O_3S$		3.8	10%	373.90

**Fig. 1** Methodology for preparation of Fe-SB

100 mL ethanol for 3 h. The product was further cleaned with DI water many times using the vacuum filter. Next, the solid was dried in the oven at 105 °C for 24 h, and labeled as sucrose biochar (SB).

$\alpha$ -FeOOH was prepared to create crystalline materials by the precipitation method. In this procedure, 50 mL of 1 M  $FeCl_3$  and 90 mL of 5 M NaOH were poured into 860 mL of DI water in a 1000 mL beaker. The mixture was then stirred using a magnetic stirrer at 250 rpm. For 5 min, the solution was carefully mixed [35]. The precipitates were aged in an oven at 70 °C for 24 h, and then, it was resuspended in DI water and centrifuged until the pH and conductivity of the supernatant solution remained constant. Subsequently, the goethite was dried at 105 °C for 24 h and denoted as  $\alpha$ -FeOOH. The reaction follows the Eq. (1):



In recent studies, researchers often focus on the performance of goethite and biochar composites with weight

ratios of 1:1 or 2:1 (goethite more than biochar), respectively [36–38]. Therefore, in this study, a new ratio of 1:4 was applied to evaluate the performance when the amount of goethite is much lower than that of biochar, positioning goethite as a supportive feature for the adsorption performance of biochar. The biochar was activated by immersing SB with  $\alpha$ -FeOOH in 20 mL of DI water (1:4, w/w), stirring for 2 h at the speed of 200 rpm, followed by oven drying at 105 °C for 24 h. Next, the product was heated to 800 °C in a muffle furnace at a rate of 10 °C/min, and the temperature was held for 2 h. After that, the solid was washed several times with DI water until the impurities were removed. Finally, the obtained biochar was placed in an oven at 60 °C for 24 h, and designated Fe-SB (Fig. 1).

### Material Characterization

Various analysis methods were used to clarify the Fe-SB characteristic. The surface morphology of Fe-SB and sucrose biochar was acquired using SEM Hitachi S-4800,

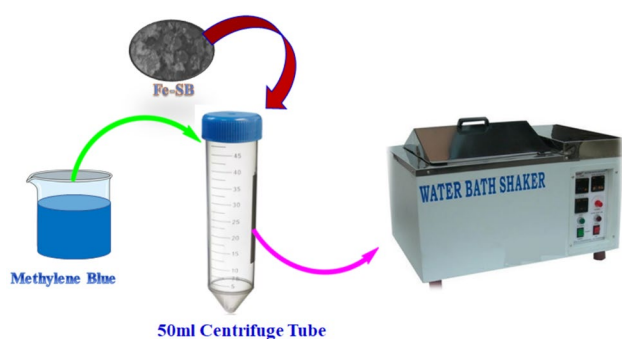


Fig. 2 Batch adsorption procedure

Japan. Brunauer–Emmett–Teller (BET) multipoint method was applied to calculate the BET surface area ( $S_{\text{BET}}$ ). The biochar was pelleted using KBr before analysis of the surface functional groups using the Fourier-transform infrared (FTIR) spectrometer PerkinElmer MIR/NIR Frontier, US. The IR spectrum was obtained and performed over the range of 400–4000  $\text{cm}^{-1}$ . The point of zero charge ( $\text{pH}_{\text{PZC}}$ ) of the Fe-SB was determined using the method described previously by Jang and Kan [39], Nguyen et al [40]. The  $\text{pH}_{\text{PZC}}$  of Fe-SB was indicated by adjusting the pH value ( $\text{pH}_{\text{Before}}$ ) of 100 mL NaCl solutions ranging from  $2.0 \pm 0.1$  to  $10 \pm 0.1$  using HCl or NaOH 0.1 M, then adding in 0.02 g Fe-SB. The mixtures were shaken for 3 h at 25 °C, then separated by filtered papers ( $\text{pH}_{\text{After}}$ ). The  $\text{pH}_{\text{PZC}}$  of Fe-SB was estimated through the plot of  $\text{pH}_{\text{Before}}$  versus the  $\Delta\text{pH} = |\text{pH}_{\text{After}} - \text{pH}_{\text{Before}}|$ .

### MB Adsorption Experiments

All MB adsorption experiments were conducted in 50 mL centrifuge tubes and shaken in an oscillation bath at room temperature (Fig. 2). For adsorption kinetic, 30 mL of MB solution with an initial concentration of 150 mg/L was poured into a tube, followed by 0.5 g/L of adsorbent. At a specified period of time, sample was taken and filtrated through a 0.45-mm Whatman® membrane filter. The residual MB concentration in filtrate was analyzed by a UV–visible spectrophotometer (Hitachi U2910) at the wavelength of 664 nm. The following equation was used to determine the adsorption capacity of Fe-SB at its equilibrium time:

$$q_e = \frac{(C_0 - C_e) \times V}{W} \quad (2)$$

where  $q_e$  (mg/g) is the MB adsorption capacity,  $C_0$  and  $C_e$  (mg/L) are the initial and equilibrium concentrations, and  $W$  (g) is the weight of Fe-SB,  $V$  (L) is the volume of the reaction solution.

Adsorption isotherms of MB onto adsorbent were investigated under an initial MB stock solution containing a range of MB concentrations (25–800 mg/L) and shaken for 7 h. To investigate the effect of pH on the adsorption capacity of adsorbent, the stock solution containing 150 mg/L of MB was pH-adjusted using 0.1 M HCl and 0.1 M NaOH to a range of 2–11. An investigation into the influence of salt on the MB adsorption on Fe-SB was carried out using a range of NaCl concentrations (0.01–1 M). Each experiment was performed in triplicate under similar conditions.

### Adsorption Kinetic and Isotherm Models

The adsorption kinetics was based on the results of the experiment on the contact time of the adsorption process. The equation of pseudo-first-order and pseudo-second-order models are presented in Eqs. (3), (4) [1]

$$\log(q_e - q_t) = \log q_e - \left( \frac{k_1}{2.303} \right) t \quad (3)$$

$$\frac{t}{q_t} = \frac{1}{k_2 q_e^2} + \frac{t}{q_e} \quad (4)$$

where  $k_1$ ,  $k_2$  are the pseudo-first and second-order constant (1/min),  $q_e$  (mg/g) is the equilibrium adsorption capacity, and  $q_t$  (mg/g) is the adsorption capacity at time  $t$  (min).

The adsorption kinetics relate to pseudo-second-order model, and an energetically heterogeneous surface frequently fits to Elovich model [41]. The diffusion of particles in the adsorption process was plotted in the intra-particle diffusion model (IPD) [42] to identify. This study calculates those two models using Eqs. (5), (6)

$$q_t = \frac{1}{\beta} \ln(\alpha\beta t + 1) \quad (5)$$

$$q_t = K_{\text{id}} t^{0.5} + C_i \quad (6)$$

where  $q_t$  (mg/g) is the adsorption capacity at time  $t$  (min).  $\alpha$  is the initial adsorption rate,  $\beta$  is the desorption constant.  $K_{\text{id}}$  is the intra-particle diffusion rate ( $\text{mg/g min}^{-0.5}$ ), and  $C_i$  offers the information about the thickness of the boundary layer.

### Adsorption Isotherm

Using the equilibrium concentration ( $C_e$ ) and equilibrium adsorption capacity ( $q_e$ ), many isotherm models were calculated. Langmuir model [43, 44] relates to some assumptions, including equivalent energy sites, monolayer adsorption, and reversible adsorption. On the other hand, the Freundlich model [45] describes a multilayer adsorption ability that is

reversible and a heterogeneous surface. Langmuir and Freundlich equation are presented in Eqs. (7) and (8)

$$q_e = \frac{K_L q_{\max} C_e}{1 + K_L C_e} \quad (7)$$

$$q_e = K_F C_e^{1/n}, \quad (8)$$

where  $q_{\max}$  (mg/g) and  $C_e$  (mg/L) are the maximum adsorption capacity and equilibrium concentration, respectively.  $K_L$  and  $K_F$  is the Langmuir constant and Freundlich constant. This parameter specifies the degree of isotherm in the following way: favorable ( $R_L < 1$ ), linear ( $R_L = 1$ ), unfavorable ( $R_L > 1$ ), or irreversible ( $R_L = 0$ ).

### Adsorption Thermodynamics

To investigate the effect of temperature on the adsorption process, changes in enthalpy ( $\Delta H^\circ$ , kJ/mol), entropy ( $\Delta S^\circ$ , kJ/mol), and Gibbs free energy ( $\Delta G^\circ$ , kJ/mol) were studied using Eqs. (9)–(12)

$$\Delta G = -RT \ln(K_c) \quad (9)$$

$$\Delta G = \Delta H^\circ - T \Delta S^\circ \quad (10)$$

$$\text{Log} K_c = \left( \frac{\Delta S^\circ}{2.303R} \right) - \left( \frac{\Delta H^\circ}{2.303RT} \right) \quad (11)$$

$$K_c = \frac{C_{Ae}}{C_e} \quad (12)$$

where  $C_e$  (mg/L) is the equilibrium concentration of MB,  $C_{Ae}$  (mg/L) is the amount of MB adsorbed on the Fe-SB per liter of solution at equilibrium.  $R$  is the universal gas constant (8.314 J/mol/K).  $K_c$  is the equilibrium constant, and  $T$  (K) is the experiment temperature. From the slope and intercept of plot  $\log K_c$  with  $1/T$ , the  $\Delta H^\circ$  and  $\Delta S^\circ$  can be calculated.

## Results and Discussion

### Characterization of Fe-SB

Through SEM analysis, Fig. 3a shows the morphology structure of SB. It can be observed that SB has a spherical structure, smooth surface, and the carbon was found to be various in size, ranging from 2 to 10  $\mu\text{m}$  [31]. This structure can offer a rigid stable skeleton and efficiently load  $\alpha$ -FeOOH nanorods on the surface. Therefore, Fig. 3b shows that the crystals of  $\alpha$ -FeOOH nanorods were well developed on the

Fe-SB surface, exhibiting a needle-like shape with lengths ranging from 5 to 10  $\mu\text{m}$ . This indicates that goethite was successfully attached to the biochar surface, enhancing its surface roughness. This result is consistent with the SEM images of  $\alpha$ -FeOOH reported in the study by Zhang et al. [46].

Figure 3c shows the FTIR spectra of the two materials in the wavenumber range from 4000  $\text{cm}^{-1}$  to 400  $\text{cm}^{-1}$ . It can be seen that the SB surface has few functional groups, because it has just undergone hydrothermal carbonization at a low temperature. On the contrary, after SB was combined with  $\alpha$ -FeOOH and heated at 800  $^\circ\text{C}$ , more diverse functional groups appeared on the surface of Fe-SB. In particular, the peaks at 3322  $\text{cm}^{-1}$  and 1157  $\text{cm}^{-1}$  of Fe-SB are related to the O–H and C–OH-stretching vibrations, respectively [47]. The peaks at 1707  $\text{cm}^{-1}$  and 1550  $\text{cm}^{-1}$  of the SB are assigned to the C=O vibration and C=C ring stretch vibrations, which reduce to a C=O peak at 1687  $\text{cm}^{-1}$  after pyrolysis to synthesize Fe-SB [47, 48]. These functional groups provide the most suitable features to enhance the MB adsorption capacity [49, 50]. Furthermore, the 636 and 555  $\text{cm}^{-1}$  peaks are related to Fe–O-stretching and Fe–OH-bending vibrations in  $\alpha$ -FeOOH that indicated the presence of  $\alpha$ -FeOOH in the Fe-SB material [46, 51].

Besides, according to the BET analysis method, the specific surface area of the Fe-SB was 568  $\text{m}^2/\text{g}$ . Materials with large specific surface areas are considered more favorable in adsorbing pollutants [52, 53]. The specific surface area of Fe-SB is significantly larger than other precursor materials like sludge-derived biochar (25  $\text{m}^2/\text{g}$ ) [54], cattle manure-derived low temperature (3.6  $\text{m}^2/\text{g}$ ) [55], and coconut fiber biochar (402.4  $\text{m}^2/\text{g}$ ) [56].

### The Adsorption of MB onto Fe-SB

pH is attributed to be an important parameter that affects the ability to adsorb contaminants in aquatic environments. Figure 4a displays the investigation of the adsorption of MB onto Fe-SB over a pH range of 2–11. The experiments were performed at an MB concentration of 40 mg/L. As can be seen, the adsorption capacity is lowest at pH-2, and then, the adsorption efficiency tends to increase gradually with the rise of pH. The adsorption capacity hits the peak at pH 8 (153 mg/g), followed by progressively decreasing to pH-11.

At low pH, poor adsorption capacity is due to  $\text{H}^+$  ions in the solution competing for adsorption sites on the biochar surface. As the pH increases, the release of  $\text{H}^+$  ions into the solution gradually decreases, and the competition steadily disappears, leading to increased adsorption capacity. The above adsorption tendency is related to the potential of the Fe-SB. Notably, the  $\text{pH}_{\text{pzc}}$  value of Fe-SB is 7.0 (Fig. 4b), which is lower than the optimal pH value of the adsorption process. When solution



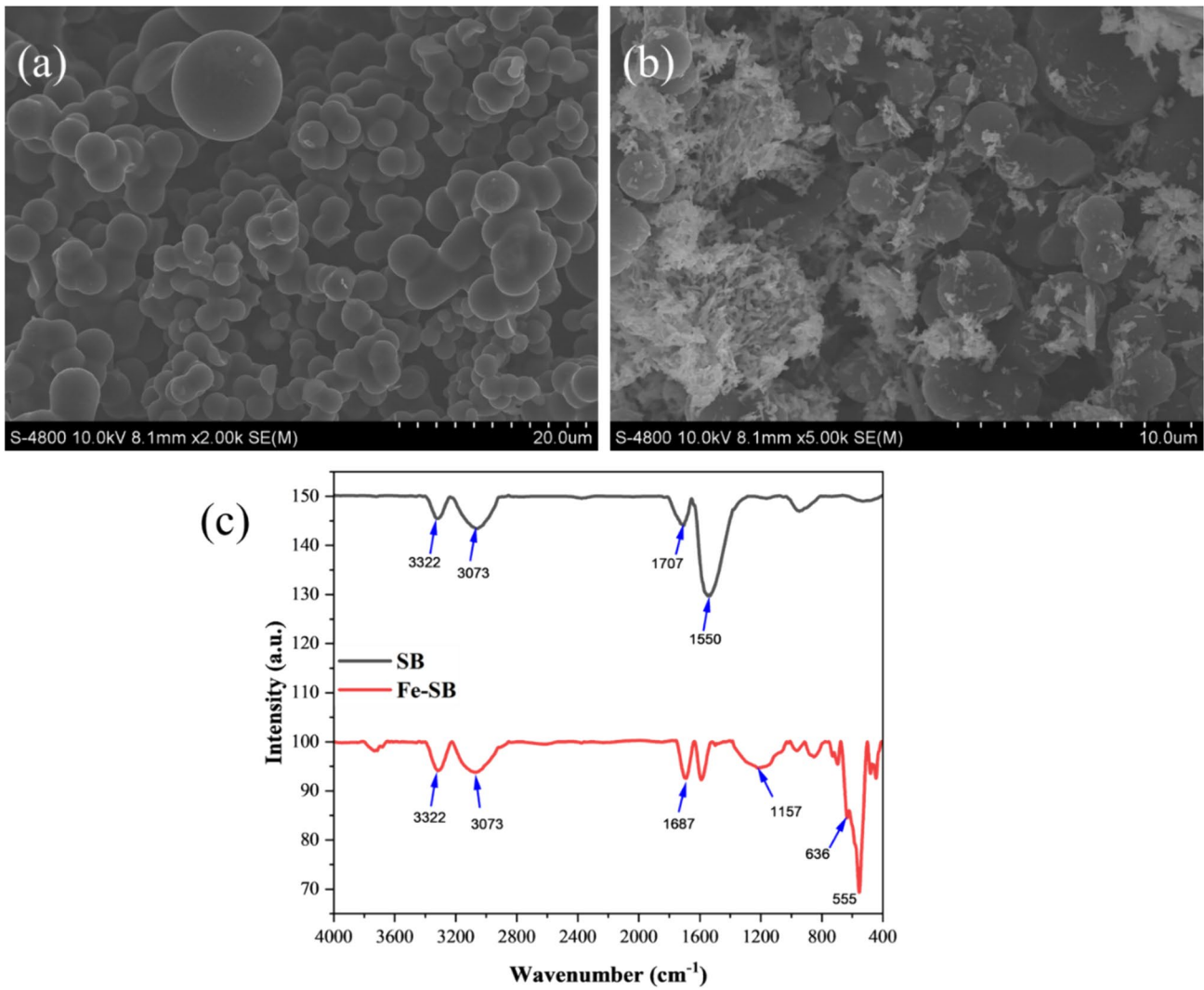


Fig. 3 SEM image of SB (a); SEM image of Fe-SB (b); FTIR analysis of Fe-SB and SB (c)

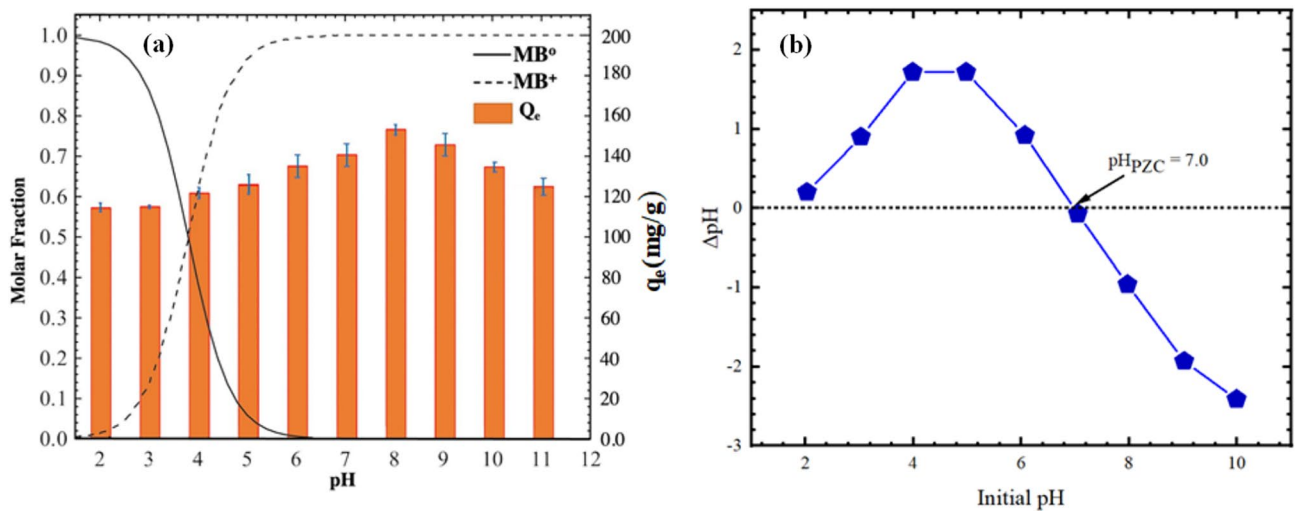


Fig. 4 The effect of initial pH on MB adsorption onto Fe-SB (a) and pH<sub>PZC</sub> (b)

$\text{pH} > \text{pH}_{\text{pzc}}$ , the cation of MB ion ( $\text{MB}^+$ ) easily binds to the negative potential surface of Fe-SB through electrostatic attraction. In addition, the strong deprotonation of the carboxyl group at neutral pH also contributes to increasing the binding of  $\text{C}=\text{O}$  on the surface of Fe-SB with MB [4]. When  $\text{pH} > 8$ , the carboxyl acid group is inhibited, and the activity of this group is reduced, leading to reduced adsorption capacity. Consequently, pH 8 was chosen as the ideal pH for the experimental condition of this research.

## Adsorption Kinetic

The kinetics models are used to represent the maximum pollutant adsorption capacity of a material in the saturated state. Data on the effect of contact time on the adsorption process were matched to pseudo-first-order, pseudo-second-order, Elovich, and intra-particle diffusion kinetic models (Fig. 5a) to identify the adsorption mechanism of Fe-SB. As shown in Table 2, the correlation factor of the Elovich model ( $R^2 = 0.9907$ ) is the highest among other models. The Elovich model describes the material as having an energetically heterogeneous surface and is involved in a second-order model associated with the nature of chemical adsorption [42, 57, 58]. Correspondingly, the model calculation of the adsorption process shows the pseudo-second-order has a high  $R^2$  (0.9438), and it pointed out that the adsorption of MB by Fe-SB is primarily classified as chemical adsorption. However, the Elovich model clarifies more information about the adsorption mechanism in this study. In addition, one stage entwined in the adsorption process usually calculated is intra-particle diffusion model. In this study, the

**Table 2** Adsorption kinetic parameters of MB

Kinetic model	Parameters	
Pseudo-first order	$q_e$ experiment	154 mg/g
	$q_e$ calculated	139 mg/g
	$K_1$	0.8466
	$R^2$	0.8987
Pseudo-second order	$q_e$ calculated	143
	$K_2$	0.00945
	$R^2$	0.9438
Elovich	A	209,243.34442
	B	0.10305
	$R^2$	0.9907
Intra Particle Diffusion	$K_{\text{diff}}$	4.02451
	C	90.57413
	$R^2$	0.5160

intra-particle diffusion model performs a  $R^2 = 0.5160$  with the adsorption process. This shows that the uptake value is more ratio with contact time than square root on time ( $t^{1/2}$ ). The chemisorption behavior of MB on goethite-based adsorbent was also found in many previous studies [59–62].

## Adsorption Isotherms

Figure 5b shows the isotherm adsorption curve using Langmuir and Freundlich models and parameters from the two models. The adsorption process takes place quickly at the initial concentration and then reaches equilibrium when raised to a high concentration. At equilibrium, the adsorption

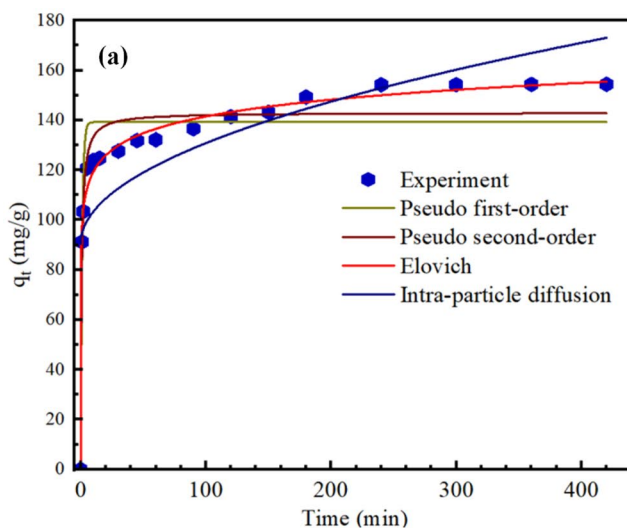
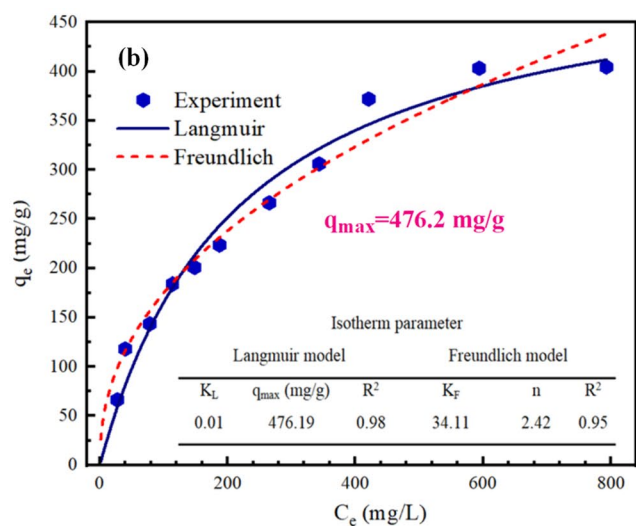


**Fig. 5** Adsorption kinetic of pseudo-first-order, pseudo-second-order, Elovich, and intra-particle diffusion (a), The Langmuir and Freundlich isotherm models to the adsorption data of MB onto the Fe-SB



(b). Experimental condition:  $[\text{Fe-SB}] = 0.5 \text{ g/L}$ ,  $\text{pH} = 8$ ,  $T = 25 \text{ }^\circ\text{C}$ ,  $[\text{MB}] = 150 \text{ mg/L}$  for adsorption kinetic, and  $[\text{MB}] = 25\text{--}800 \text{ mg/L}$  for adsorption isotherm

capacity is 476.2 mg/g, based on the Langmuir model. In the Freundlich model, the  $1/n$  parameter was less than one, indicating the occurrence of a chemisorption interaction [42]. Recognizably, two models have the experiment data with a high  $R^2$  ( $> 0.95$ ). This result shows the assumption involving two models appears in the adsorption process in this study, demonstrating that the adsorption process of MB on Fe-SB occurs simultaneously with monolayer and multilayer adsorption. H-bonding, electron donor and acceptor, and  $\pi$ - $\pi$  interaction are the main mechanisms contributing to the isothermal adsorption of Fe-SB. When compared with previous research results, the maximum adsorption capacity of MB on Fe-SB was higher than that of other adsorbents (Table 3).

### Adsorption Thermodynamics

The thermodynamic characteristics of MB adsorption on Fe-SB were described using the thermodynamic factors of free energy change  $\Delta G^o$  (KJ/mol), enthalpy change  $\Delta H^o$  (KJ/mol), and entropy change  $\Delta S^o$  (J/K.mol). Table 4 displays the thermodynamic factors of MB adsorption. The heat-releasing and spontaneous nature of the adsorption process is indicated by the negative  $\Delta H$  and positive  $\Delta G$  [67]. As the temperature of adsorption increases, the adsorption capacity also increases. The values of  $\Delta G$  for the adsorption of MB onto Fe-SB were determined at 283 K, 304 K, and 315 K. It was observed that  $\Delta G$  decreases as the temperature increases, suggesting that adsorption becomes more

favorable at higher temperatures, and the MB adsorption on Fe-SB is thermodynamically spontaneous [68]. A strong interaction between the adsorbate and adsorbent is described by the high value of  $\Delta H$  [69]. The value of  $\Delta H < 0$  suggests an exothermic adsorption process. The positive values of  $\Delta S$  indicate an increase in casualness at the solid/solution interface throughout the adsorption process [67].

### Effect of Salts on MB Adsorption and Application to Actual Samples

The effluents from textile industries contain a considerable quantity of salts. Therefore, it is essential to investigate the impact of salt on the adsorption process. The presence of salt in the aqueous solution is attributed to hindering the binding affinity between the adsorbent surface and the MB, which ultimately influences the capacity of adsorption [70]. The effect of salts on MB adsorption has been examined using sodium chloride (NaCl) salt (Fig. 6a). The finding indicated that the presence of NaCl salt resulted in a reduction in the MB dye removal capacity.

The study utilized four water sources, including DI, tap, ground, and river water, to evaluate the selectivity of adsorbent toward MB in the adsorption process. As expected, the adsorption capacity of Fe-SB decreases in the order of DI (206.29 mg/g) > tap (88.98 mg/g) > ground (81.39 mg/g) > river (80.58 mg/g) (Fig. 6b). Furthermore, the conductivity of the water samples increases in the

**Table 3** Maximum adsorption capacity ( $q_{max}$ ) data for MB documented in the literature

Adsorbents	pH	Pyrolysis conditions	Initial MB (mg/L)	Volume (mL)	Biochar dosage (g/L)	$q_{max}$ (mg/g)	Reference
Activated carbon	7	110 °C 6 h	100	10	0.04	58.14	[63]
The biochar derived from <i>Cedrela odorata</i> seeds	any pH	400 °C 1 h	100	25	0.03	158.8	[64]
Eucalyptus camdulensis biochar	6	800 °C 3 h	100	100	0.3	123.3	[65]
Biochar derived from Cattle manure	3–4	200 °C 0.5 h	200	20	0.05	241.99	[55]
Sludge-based biochar	11	550 °C 24 h	50 -100	20	6.0	24.10	[54]
Sludge-based magnetic biochar	12–14	750 °C 2 h	50	20	5.0	50	[66]
Olive stone	8–10	110 °C 24 h	20	50	0.2	44.5	[2]
Spherical Carbon	any pH	190 °C 11 h	300–900	25	0.8	713.94	[31]
<b>Fe-SB</b>	8	800 °C 1 h	25–800	30	0.5	<b>476.2</b>	<b>This study</b>

Fe-SB: Modified Sucrose Biochar Goethite ( $\alpha$ -FeOOH), MB: Methylene Blue

**Table 4** Thermodynamics parameters for MB adsorption on Fe-SB

Temp (K)	$K_L$	$\Delta G^o$ (KJ /mol)	$\Delta H^o$ (KJ /mol)	$\Delta S^o$ (J/K.mol)	$R^2$
283	242,325.30	-29.17	-2.96	1.81	0.9876
304	124,487.70	-29.65			
315	81,304.77	-29.60			



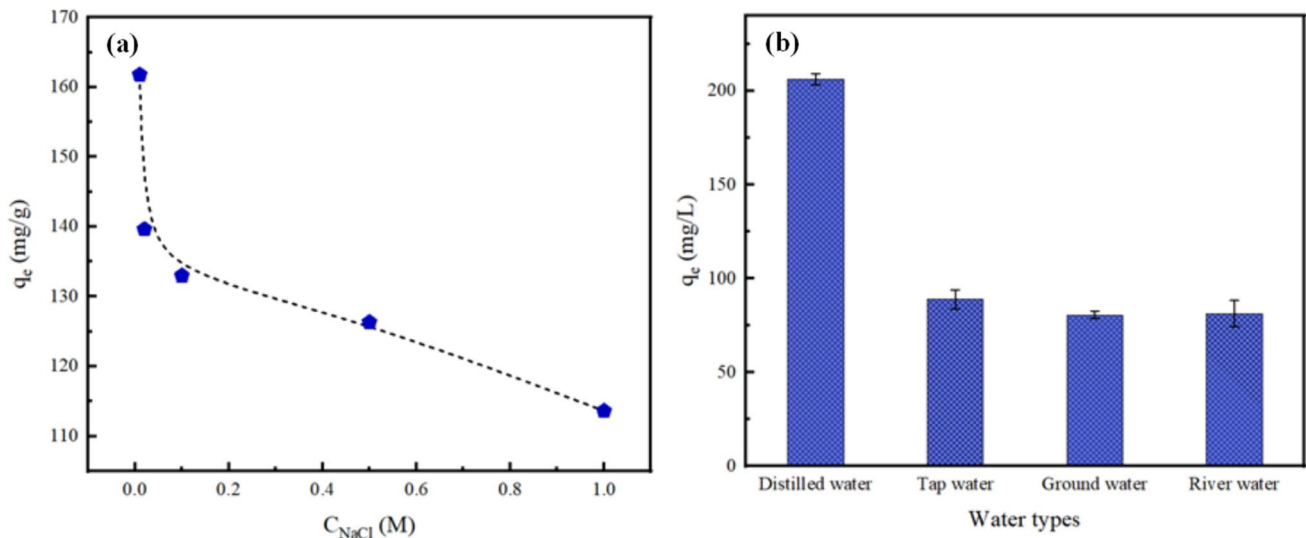


**Fig. 6** Effect of salts on MB adsorption (a) and application to actual samples (b)

same order: DI ( $0.42 \mu\text{S}/\text{cm}$ ) < tap ( $2.65 \mu\text{S}/\text{cm}$ ) < ground ( $11.63 \mu\text{S}/\text{cm}$ ) < river ( $17.96 \mu\text{S}/\text{cm}$ ). This indicates that the presence of water-soluble substances affects the adsorption capacity of MB on the Fe-SB material, leading to competition between MB and soluble substances that are available in the water sources. Specifically, as the conductivity increases, the adsorption capacity decreases.

### Adsorption Mechanism

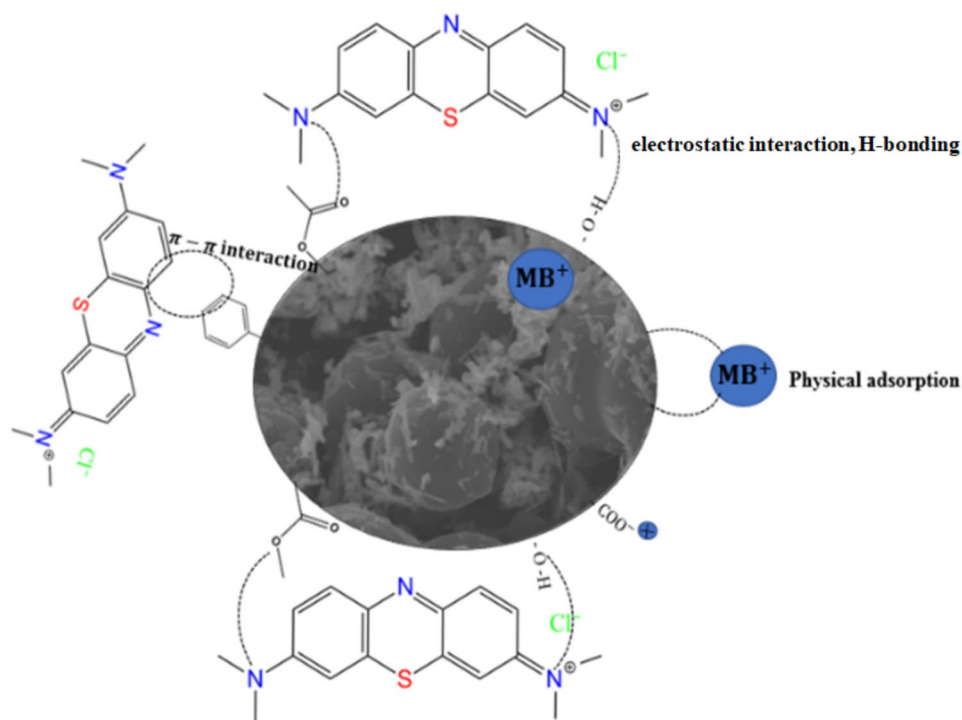
Figure 7 summarizes the adsorption mechanism of MB onto Fe-SB. The adsorption mechanism was thoroughly discovered based on the characterization and the outcomes of adsorption tests. The efficient adsorption of MB was attributed to the high specific surface area and abundant pore structure of Fe-SB. The combination of hydrochar with  $\alpha$ -FeOOH before high-temperature pyrolysis improved the properties of the material, resulting in an increase in the specific surface area of the material ( $568 \text{ m}^2/\text{g}$ ). The large specific surface area stimulates Fe-SB to attract MB molecules embedded in the material, contributing to the physisorption mechanism [71]. FTIR spectra suggested that O–H functional group on Fe-SB, and nitrogen and oxygen-containing group of MB formed H-bonding [72]. In addition, Fe-SB contains C=C aromatic ring ready to act as a  $\pi$ -electron donor, and MB could act as a  $\pi$ -electron acceptor due to the strong electron attraction ability of the benzene ring of MB. The connection between these two  $\pi$  electrons promotes Fe-SB to adsorb MB through the  $\pi$ – $\pi$  interaction mechanism

[67]. Furthermore, the adsorption capacity of Fe-SB for MB was enhanced by the electrostatic interaction mechanism between the negative charge of Fe-SB and MB cations in solution at high pH. With the synergistic effect of these mechanisms, not only Fe-SB but also other goethite-based materials can be utilized to treat various pollutants beyond MB, such as Congo Red [73], Methyl Orange [74], or even heavy metals like Copper and Cadmium [75]. Notably, in the study by Ugbe and Abdus-Salam [59], it was demonstrated that the adsorption of MB on goethite nanoparticles can be reversed by decreasing the pH through acid addition with very low acid concentration. MB was completely desorbed, independent of the adsorbent, laying the foundation for multiple reuse cycles.

### Conclusions

In this study, a novel Fe-SB biochar derived from sucrose was modified for synthesis via hydrothermal coupling with goethite. The obtained biochar exhibited a large specific surface area and abundance of functional groups and unveiled an outstanding result of Langmuir adsorption capacity ( $476.2 \text{ mg}/\text{g}$ ) at pH 8. Physisorption, H-bonding, electrostatic interaction, and  $\pi$ – $\pi$  interaction are the major adsorption mechanisms between Fe-SB and MB. Overall, the Fe-SB in this research was revealed to be an environmentally friendly and potential adsorbent for MB removal in water remediation.

**Fig. 7** Proposed adsorption mechanism of MB by Fe-SB



**Acknowledgements** The authors would like to thank researchers from various universities for their collaboration. The authors would also like to thank Miss. Thuy-Van Tran, Miss. Yen-Nhi-Nguyen Tran, and Mrs Nhu-Thuan Pham for sample collecting throughout the study.

**Author Contributions** Investigation, software, and writing original draft & editing: Van-Truc Nguyen; software and writing original draft: Quoc-Hoang Do and Vu-Anh Le; data curation, conceptualization, and methodology: Anh Thi Kim Tran and My Linh Nguyen; Formal analysis and investigation: Quoc-Minh Truong; writing—review & editing: Thanh-Binh Nguyen, Nhung Thi-Tuyet Hoang, and Tran Thi Ai My; supervision, and writing—review & editing: Nguyen Duy Dat and Thi-Dieu-Hien Vo.

**Funding** The authors did not receive support from any organization for the submitted work.

**Data availability** The authors declare that the data supporting the findings of this study are available within the paper and its Supplementary Information files.

## Declarations

**Conflict of interest** The authors have no relevant financial or non-financial interests to disclose.

## References

- B.T. Gemici, H.U. Ozel, H.B. Ozel, *Environ. Technol. Innov.* (2021). <https://doi.org/10.1016/j.eti.2021.101501>
- S.M. Alardhi, H.G. Salih, N.S. Ali, A.H. Khalbas, I.K. Salih, N.M.C. Saady, S. Zendejboudi, T.M. Albayati, H.N. Harharah, *Sci. Rep.* (2023). <https://doi.org/10.1038/s41598-023-47319-x>
- M. Al-Mamun, S. Kader, M. Islam, M. Khan, *J. Environ. Chem. Eng.* (2019). <https://doi.org/10.1016/j.jece.2019.103248>
- E. Alver, A.Ü. Metin, F. Brouers, *Int. J. Biol. Macromol.* (2020). <https://doi.org/10.1016/j.ijbiomac.2020.02.330>
- M. Berradi, R. Hsissou, M. Khudhair, M. Assouag, O. Cherkaoui, A. El Bachiri, A. El Harfi, *Heliyon* (2019). <https://doi.org/10.1016/j.heliyon.2019.e02711>
- R.H. Khudhur, N.S. Ali, E.H. Khader, N.S. Abbood, I.K. Salih, T.M. Albayati, *Desalin. Water Treat.* (2023). <https://doi.org/10.5004/dwt.2023.29861>
- A.E. Mahdi, N.S. Ali, K.R. Kalash, I.K. Salih, M.A. Abdulrahman, T.M. Albayati, *Prog. Color Color. Coat.* (2023). <https://doi.org/10.3009/pccc.2023.167111.1205>
- T.M. Dao, T. Le Luu, *Bioresour. Technol. Rep.* (2020). <https://doi.org/10.1016/j.biteb.2020.100583>
- S.S. Auerbach, D.W. Bristol, J.C. Peckham, G.S. Travlos, C.D. Hébert, R.S. Chhabra, *Food Chem. Toxicol.* (2010). <https://doi.org/10.1016/j.fct.2009.09.034>
- S. Widarti, Y. Suprianti, A.S. Kurniasetiawati, R.I. Tritjahjono, *ASEAN J. Chem.* (2023). <https://doi.org/10.22146/ajche.78794>
- S.M. Alardhi, N.S. Ali, N.M.C. Saady, S. Zendejboudi, I.K. Salih, J.M. Alrubaye, T.M. Albayati, *J. Ind. Eng. Chem.* (2024). <https://doi.org/10.1016/j.jiec.2023.09.051>
- N.S. Ali, K.R. Kalash, A.N. Ahmed, T.M. Albayati, *Sci. Rep.* (2022). <https://doi.org/10.1038/s41598-022-20984-0>
- T.M. Albayati, A.M. Doyle, *Int. J. Chem. React. Eng.* (2014). <https://doi.org/10.1515/ijcre-2013-0120>
- T.M. Albayati, A.M. Doyle, *J. Nanopart. Res.* (2015). <https://doi.org/10.1007/s11051-015-2924-6>
- N. Ahmad, M.I. Nabeel, S.J. Ali, B. Fatima, H.N. Rashid, M. Najam-ul-Haq, S.G. Musharraf, D. Hussain, *Sustain. Mater. Technol.* (2023). <https://doi.org/10.1016/j.susmat.2023.e00698>

16. C.R. Holkar, A.J. Jadhav, D.V. Pinjari, N.M. Mahamuni, A.B. Pandit, J. Environ. Manag. (2016). <https://doi.org/10.1016/j.jenvman.2016.07.090>
17. Y. Zhang, Y. Zheng, Y. Yang, J. Huang, A.R. Zimmerman, H. Chen, X. Hu, B. Gao, Bioresour. Technol. (2021). <https://doi.org/10.1016/j.biortech.2021.125432>
18. N.S. Ali, H.N. Harharah, I.K. Salih, N.M. Cata Saady, S. Zendejboudi, T.M. Albayati, Sci. Rep. (2023). <https://doi.org/10.1038/s41598-023-37090-4>
19. A. Mahdi, N. Ali, H.S. Majdi, T.M. Albayatia, M. Abdulrahman, D. Jasim, K. Kalash, I. Salih, Desalin. Water Treat. (2023). <https://doi.org/10.5004/dwt.2023.29741>
20. S. Altenor, B. Carene, E. Emmanuel, J. Lambert, J.-J. Ehrhardt, S. Gaspard, J. Hazard. Mater. (2009). <https://doi.org/10.1016/j.jhazmat.2008.10.133>
21. B. Hameed, A.M. Din, A. Ahmad, J. Hazard. Mater. (2007). <https://doi.org/10.1016/j.jhazmat.2006.07.049>
22. M. Ghaedi, A.G. Nasab, S. Khodadoust, M. Rajabi, S. Azizian, J. Ind. Eng. Chem. (2014). <https://doi.org/10.1016/j.jiec.2013.10.007>
23. L. Lonappan, T. Rouissi, R.K. Das, S.K. Brar, A.A. Ramirez, M. Verma, R.Y. Surampalli, J.R. Valero, Waste Manag. (2016). <https://doi.org/10.1016/j.wasman.2016.01.015>
24. H.J. Al-Jaaf, N.S. Ali, S.M. Alardhi, T.M. Albayati, Desalin. Water Treat. (2022). <https://doi.org/10.5004/dwt.2022.27986>
25. Q. Qian, M. Machida, M. Aikawa, H. Tatsumoto, J. Mater. Cycles Waste Manag. (2008). <https://doi.org/10.1007/s10163-007-0185-x>
26. Q. Qian, S. Sunohara, Y. Kato, M.A.A. Zaini, M. Machida, H. Tatsumoto, Appl. Surf. Sci. (2008). <https://doi.org/10.1016/j.apsusc.2008.01.111>
27. D.C. Tsang, F. Zhou, W. Zhang, R. Qiu, Chemosphere (2016). <https://doi.org/10.1016/j.chemosphere.2016.01.060>
28. Q. Miao, Y. Tang, J. Xu, X. Liu, L. Xiao, Q. Chen, J. Taiwan Inst. Chem. Eng. (2013). <https://doi.org/10.1016/j.jtice.2012.12.006>
29. Y. Shi, X. Zhang, G. Liu, ACS Sustain. Chem. Eng. (2015). <https://doi.org/10.1021/acssuschemeng.5b00670>
30. J. Chung, N. Sharma, M. Kim, K. Yun, J. Water Process. Eng. (2022). <https://doi.org/10.1016/j.jwpe.2022.102763>
31. K.C. Bedin, A.C. Martins, A.L. Cazetta, O. Pezoti, V.C. Almeida, Chem. Eng. J. (2016). <https://doi.org/10.1016/j.cej.2015.10.099>
32. P. Ouředníček, B. Hudcová, L. Trakal, M. Pohořelý, M. Komárek, Sci. Total. Environ. (2019). <https://doi.org/10.1016/j.scitotenv.2019.03.300>
33. A. Hsini, M. Benafqir, Y. Naciri, M. Laabd, A. Bouziani, M. Ezzahery, R. Lakhmiri, N.E. Alem, A. Albourine, Colloids Surf A Physicochem Eng Asp (2021). <https://doi.org/10.1016/j.colsurfa.2021.126274>
34. S. Zhang, Q. Du, Y. Sun, J. Song, F. Yang, D.C.W. Tsang, Sci. Total. Environ. (2020). <https://doi.org/10.1016/j.scitotenv.2020.137415>
35. M. Zhang, B. Gao, S. Varnoosfaderani, A. Hebard, Y. Yao, M. Inyang, Bioresour. Technol. (2013). <https://doi.org/10.1016/j.biortech.2012.11.132>
36. Y. Wang, S. Joseph, C. Chen, X. Qi, D.R.G. Mitchell, H. Si, J. Shang, Chem. Eng. J. (2023). <https://doi.org/10.1016/j.cej.2023.146542>
37. F. Yang, S. Zhang, H. Li, S. Li, K. Cheng, J.-S. Li, D.C.W. Tsang, Chem. Eng. J. (2018). <https://doi.org/10.1016/j.cej.2018.04.161>
38. Y. Yu, Z. Zhong, H. Guo, Y. Yu, T. Zheng, H. Li, Z. Chang, Sci. Total. Environ. (2023). <https://doi.org/10.1016/j.scitotenv.2022.159940>
39. H.M. Jang, E. Kan, Bioresour. Technol. (2019). <https://doi.org/10.1016/j.biortech.2018.11.081>
40. V.T. Nguyen, T.B. Nguyen, C.P. Huang, C.W. Chen, X.T. Bui, C.D. Dong, J. Water Process. Eng. (2021). <https://doi.org/10.1016/j.jwpe.2020.101908>
41. C.W. Cheung, J.F. Porter, G. McKay, Water Res. (2001). [https://doi.org/10.1016/S0043-1354\(00\)00306-7](https://doi.org/10.1016/S0043-1354(00)00306-7)
42. T.R. Sahoo, B. Prelot, in *Nanomaterials for the detection and removal of wastewater pollutants*. ed. by B. Bonelli, F.S. Freyria, I. Rossetti, R. Sethi (Elsevier, Amsterdam, 2020), pp.161–222
43. I. Langmuir, J. Am. Chem. Soc. (1916). <https://doi.org/10.1021/ja02268a002>
44. I. Langmuir, J. Am. Chem. Soc. (1917). <https://doi.org/10.1021/ja02254a006>
45. H.M.F. Freundlich, J. Phys. Chem. **57**, 385–471 (1906)
46. L. Zhang, F. Fu, B. Tang, Chem. Eng. J. (2019). <https://doi.org/10.1016/j.cej.2018.08.224>
47. Q. Chen, Q. Wu, J. Hazard. Mater. (2015). <https://doi.org/10.1016/j.jhazmat.2014.09.024>
48. M. Wortmann, W. Keil, B. Brockhagen, J. Biedinger, M. Westphal, C. Weinberger, E. Diestelhorst, W. Hachmann, Y. Zhao, M. Tiemann, G. Reiss, B. Hüsgen, C. Schmidt, K. Sattler, N. Frese, J. Anal. Appl. Pyrol. (2022). <https://doi.org/10.1016/j.jaap.2021.105404>
49. R. Han, Y. Wang, P. Han, J. Shi, J. Yang, Y. Lu, J. Hazard. Mater. (2006). <https://doi.org/10.1016/j.jhazmat.2006.02.029>
50. D. Kavitha, C. Namasivayam, Bioresour. Technol. (2007). <https://doi.org/10.1016/j.biortech.2005.12.008>
51. I. Andjelkovic, D.N.H. Tran, S. Kabiri, S. Azari, M. Markovic, D. Losic, ACS Appl. Mater. Interfaces (2015). <https://doi.org/10.1021/acsami.5b01624>
52. G. Tan, W. Sun, Y. Xu, H. Wang, N. Xu, Bioresour. Technol. (2016). <https://doi.org/10.1016/j.biortech.2016.03.147>
53. T.M.N. Albayati, S.E. Wilkinson, A.A. Garforth, A.M. Doyle, Transp. Porous Media (2014). <https://doi.org/10.1007/s11242-014-0336-1>
54. S. Fan, Y. Wang, Z. Wang, J. Tang, J. Tang, X. Li, J. Environ. Chem. Eng. (2017). <https://doi.org/10.1016/j.jece.2016.12.019>
55. Y. Zhu, B. Yi, Q. Yuan, Y. Wu, M. Wang, S. Yan, RSC Adv. (2018). <https://doi.org/10.1039/C8RA03018A>
56. Q.A. Binh, P. Kajitvichyanukul, Water Sci. Technol. (2019). <https://doi.org/10.2166/wst.2018.529>
57. C. Aharoni, F.C. Tompkins, in *Advances in catalysis*. ed. by D.D. Eley, H. Pines, P.B. Weisz (Academic Press, Cambridge, 1970), pp.1–49
58. R.-S. Juang, M.-L. Chen, Ind. Eng. Chem. Res. (1997). <https://doi.org/10.1021/ie960351f>
59. F.A. Ugbe, N. Abdus-Salam, Arab J Chem Environ. (2020) <https://www.mocedes.org/ajcer-volume8/volume7/AJ CER-02-Ugbe-2020.pdf>
60. N. Abdus-Salam, F.A. Ugbe, V.A. Ikudayisi-Ugbe, Songklanakarin J Sci Technol. (2022) <https://sjst.psu.ac.th/journal/44-2/7.pdf>
61. N. Abdus-Salam, V. Ikudayisi, Ife J Sci. (2017). <https://doi.org/10.4314/ijjs.v19i1.10>
62. N. Abdus-Salam, A.V. Ikudayisi-Ugbe, F.A. Ugbe, Acta Sci Malays. (2021). <https://doi.org/10.26480/asm.01.2021.27.35>
63. A. Inengite, C. Abasi, D. Johnny, Environ. Nat. Resour. J. (2014). <https://doi.org/10.5539/enrr.v4n4p120>
64. A. Subratti, J.L. Vidal, L.J. Lalgee, F.M. Kerton, N.K. Jalsa, Sustain. Chem. Pharm. (2021). <https://doi.org/10.1016/j.scp.2021.100421>
65. M.T. Amin, A.A. Alazba, M. Shafiq, Sustainability (2021). <https://doi.org/10.3390/su13073600>
66. N. Chaukura, E.C. Murimba, W. Gwenzi, Environ. Technol. Innov. (2017). <https://doi.org/10.1016/j.eti.2017.06.004>
67. S. Fan, J. Tang, Y. Wang, H. Li, H. Zhang, J. Tang, Z. Wang, X. Li, J. Mol. Liq. (2016). <https://doi.org/10.1016/j.molliq.2016.04.107>
68. L. Leng, X. Yuan, H. Huang, J. Shao, H. Wang, X. Chen, G. Zeng, Appl. Surf. Sci. (2015). <https://doi.org/10.1016/j.apsusc.2015.04.014>
69. L. Shi, G. Zhang, D. Wei, T. Yan, X. Xue, S. Shi, Q. Wei, J. Mol. Liq. (2014). <https://doi.org/10.1016/j.molliq.2014.07.023>

70. S. Afroze, T.K. Sen, M. Ang, H. Nishioka, Desalin. Water Treat. (2016). <https://doi.org/10.1080/19443994.2015.1004115>
71. S. Singh, A.K. Prajapati, J.P. Chakraborty, M.K. Mondal, Biomass Convers. Biorefin. (2021). <https://doi.org/10.1007/s13399-021-01645-0>
72. M. Almarri, X. Ma, C. Song, Energy Fuel (2009). <https://doi.org/10.1021/ef900051r>
73. C.C. Ong, R. Jose, M.S.M. Saheed, Chem. Eng. J. (2020). <https://doi.org/10.1016/j.cej.2020.124306>
74. V.S. Munagapati, V. Yarramuthi, D.-S. Kim, J. Mol. Liq. (2017). <https://doi.org/10.1016/j.molliq.2017.05.099>
75. A. Jaiswal, S. Banerjee, R. Mani, M.C. Chattopadhyaya, J. Environ. Chem. Eng. (2013). <https://doi.org/10.1016/j.jece.2013.05.007>

**Publisher's Note** Springer Nature remains neutral with regard to jurisdictional claims in published maps and institutional affiliations.

Springer Nature or its licensor (e.g. a society or other partner) holds exclusive rights to this article under a publishing agreement with the author(s) or other rightsholder(s); author self-archiving of the accepted manuscript version of this article is solely governed by the terms of such publishing agreement and applicable law.